EFIT tokamak equilibria with toroidal flow and anisotropic pressure using the two-temperature guiding-centre plasma

Michael Fitzgerald

Research School of Physical Sciences and Engineering, Australian National University, 0200 ACT, Australia

Lynton Appel

EURATOM/CCFE Fusion Association, Culham Science Centre, Abingdon, Oxfordshire, OX14 3DB, UK

Matthew Hole

Research School of Physical Sciences and Engineering, Australian National University, 0200 ACT, Australia

Abstract

A new force balance model for the EFIT [1] magnetohydrodynamic equilibrium technique for tokamaks is presented which includes the full toroidal flow and anisotropy changes to the Grad-Shafranov equation. The free functions are one dimensional poloidal flux functions and all non-linear contributions to the toroidal current density are treated iteratively. The parallel heat flow approximation chosen for the model is that parallel temperature is a flux function and that both parallel and perpendicular pressures may be described using parallel and perpendicular temperatures. This choice for the fluid thermodynamics has been shown elsewhere [2] to be the same as a guiding centre kinetic solution of the same problem under the same assumptions. The model reduces identically to the static and isotropic Grad-Shafranov equation in the appropriate limit as different flux functions are set to zero. An analytical solution based on a modified Soloviev solution for non-zero toroidal flow and anisotropy is also presented.

The force balance model has been demonstrated in the code EFIT TENSOR by modifying an existing code EFIT++ [3]. Benchmark results for EFIT TENSOR are presented and the more complicated force balance model is found to converge to force balance similarly to the usual EFIT model and with comparable speed.

Keywords: tokamak, equilibrium, EFIT, reconstruction, flow, anisotropy, MHD, magnetohydrodynamics, nuclear, fusion, plasma, fast particles, NBI, ICRH

1. Introduction

The macroscopic equations of magnetohydrodynamics (MHD) provide the basic starting point for an understanding of plasma physics in a modern tokamak experiment. Good knowledge of the total equilibrium force balance provides information about the magnetic topology and the plasma thermodynamic variables so that more detailed stability and transport treatments can be pursued. The success of the tokamak concept has been possible, in part, due to the simple models which support inference of the plasma configuration from incomplete measurements of related parameters. Most basic physical variables can only be measured indirectly on a fusion experiment through a sophisticated and expensive set of diagnostics. Good physical models of the configuration are essential, particularly for future power stations which cannot accommodate complex diagnostics programmes.

Modern tokamak experiments contain a significant portion of fast ions [4] resulting from heating processes such as neutral beam injection (NBI) and ion-cyclotron resonance heating (ICRH) which can rotate the plasma and also produce highly

Email address: Michael.Fitzgerald@anu.edu.au (Michael Fitzgerald)

anisotropic fast particle pressures [5, 6]. Both of these effects can move the plasma off magnetic field surfaces and significantly alter the density profile and magnetic topology (see, for example, [2, 7, 8, 9, 10]).

The tokamak equilibrium reconstruction code EFIT [1] has served as the de-facto standard technique to infer equilibrium from experimental diagnostics and there have been many different code implementations of this technique. EFIT solves the MHD force balance for a static and isotropic pressure, although approximate inclusions of toroidal flow [3] and anisotropy [11] exist in some versions through modifications to pressure function.

In this paper, we describe an extension of the basic EFIT algorithm to include the fully non-linear toroidal flow and anisotropy contributions to the 2-D plasma equilibrium problem. The physical model is based on the guiding-centre plasma (GCP) formalism [12] as derived by Dobrott and Greene [13] for a two-temperature anisotropic plasma model [2]. This new algorithm has been demonstrated in EFIT TENSOR, a code created by modifying an existing EFIT implementation used currently for the MAST tokamak (known as 'EFIT++' [3]). We will present analytical and MAST test case equilibria produced by EFIT TENSOR and demonstrate correct numerical convergence to force balance.

2. Basic equations and assumptions

We are concerned with the system of macroscopic equilibrium equations, based on the guiding-centre plasma and the MHD Ohm's law, given in natural units as [12, 13]

$$\rho(\mathbf{u}\cdot\nabla\mathbf{u}) + \nabla\cdot\overleftrightarrow{P} = \mathbf{J}\times\mathbf{B} \tag{1}$$

$$\overleftrightarrow{P} = p_\perp\overleftrightarrow{I} + \Delta\mathbf{B}\mathbf{B}, \Delta \equiv \frac{p_\parallel - p_\perp}{B^2} \tag{2}$$

$$\nabla\cdot\mathbf{B} = 0 \tag{3}$$

$$\nabla\cdot\rho\mathbf{u} = 0 \tag{4}$$

$$\nabla\times\mathbf{B} = \mathbf{J} \tag{5}$$

$$\mathbf{E} + \mathbf{u}\times\mathbf{B} = 0 \tag{6}$$

$$\nabla\times\mathbf{E} = 0 \tag{7}$$

The single fluid pressure dyad $\overleftrightarrow{P}$ and its components $p_\parallel, p_\perp$, the single fluid velocity u and single fluid mass density ρ have textbook definitions (e.g.: [14]) in terms of each individual fluid equation for each species present in the plasma, which in turn are moments of the guiding centre plasma model for each species. Divergence-less quantities (Eqs. (3) and (4)) in a 2-d axisymmetric cylindrical system (R, ϕ, Z) permit the covariant representations

$$\mathbf{B} = \nabla\psi\times\nabla\phi + RB_\phi\nabla\phi \tag{8}$$

$$\rho\mathbf{u} = \nabla\psi_M\times\nabla\phi + R\rho u_\phi\nabla\phi \tag{9}$$

in terms of poloidal stream functions ψ and ψ_M. Combining Eqs. (8) and (9) with Eqs. (6) and (7) gives the well-known 'frozen-in' condition for magnetic field lines in axisymmetric cylindrical geometry

$$\mathbf{u} = \frac{\psi_M'(\psi)}{\rho}\mathbf{B} + R^2\Omega(\psi)\nabla\phi \tag{10}$$

which specifies that, to conserve magnetic flux through a given fluid element, all macroscopic ideal flow must occur parallel to the magnetic field or in a symmetry direction. Under these assumptions, flow in a poloidal direction can only manifest as the projection of flow in the parallel direction and toroidal angular velocity Ω is constant on poloidal flux surfaces. In this study, we neglect all poloidal flows setting $\psi_M'(\psi) = 0$.

To close the system of equations, an energy equation is required. Ignoring resistivity or other dissipation, the work done against the pressure equals the change in plasma energy U for a reversible process

$$\overleftrightarrow{P}:\nabla\mathbf{u} = \frac{p_\parallel}{\rho}\frac{d\rho}{dt} - \Delta B\frac{dB}{dt} = \rho\frac{dU}{dt} \tag{11}$$

(noting that under most circumstances in this work, we will keep all thermodynamic quantities in units of energy density per unit mass). In the guiding centre model, relationships between the moments of the distribution function are obtained from a kinetic equation [12]. These relationships depend on the form of the distribution function rather than the macroscopic variables alone, which is inconvenient for a fluid description. However, a thermodynamic statement can be reconciled [2, 15] with the kinetic model and give the same results for certain simple choices of the functional form of the macroscopic variables. For example, an isotropic Maxwellian distribution, $p = \rho T(\psi)$, gives identical results in both models. In this study, our GCP compatible choice is to assume a two-temperature Maxwellian distribution of the form

$$p_\parallel(\rho, B, \psi) = \rho T_\parallel(\psi) \tag{12}$$

$$p_\perp(\rho, B, \psi) = \rho T_\perp(B, \psi) \tag{13}$$

3. Grad-Shafranov equation with toroidal flow and anisotropy

Many examples of the Grad-Shafranov equation exist for static [16], anisotropic [17, 11, 10], and flowing [18, 19, 20, 21] equilibria. An equation incoporating both flow and anisotropy [2, 15] is used in this study and is outlined in this section. Various reductions of this general case to other known forms are given in the appendix.

The basic scalar equations for force balance are obtained from components of Eq. (1). The toroidal component of force balance yields a new flux function $F(\psi)$ for the toroidal magnetic field

$$F(\psi) = (1-\Delta)RB_\phi \tag{14}$$

the parallel component of force balance gives a Bernoulli equation and new flux function $H(\psi)$

$$H(\psi) = W(\rho, B, \psi) - \frac{1}{2}R^2\Omega(\psi)^2 \tag{15}$$

$$W(\rho, B, \psi) \equiv U + \frac{p_\parallel}{\rho} \tag{16}$$

written in terms of a Legedre transform from energy U to enthalpy W in Eq. (16). Finally, we recover a modified Grad-Shafranov equation from the ψ component of force balance

$$\begin{aligned} \nabla\cdot\left[(1-\Delta)\left(\frac{\nabla\psi}{R^2}\right)\right] = \\ -\rho T_\parallel'(\psi) - \rho H'(\psi) \\ +\rho\left(\frac{\partial W}{\partial\psi}\right)_{B,\rho} - \frac{F(\psi)F'(\psi)}{R^2(1-\Delta)} + \rho R^2\Omega(\psi)\Omega'(\psi) \end{aligned} \tag{17}$$

subject to the integrability conditions constrained by energy conservation (Eq. (11))

$$\left(\frac{\partial W}{\partial\rho}\right)_{B,\psi} = \frac{1}{\rho}\left(\frac{\partial p_\parallel}{\partial\rho}\right)_{B,\psi} \tag{18}$$

$$\left(\frac{\partial W}{\partial B}\right)_{\rho,\psi} = \frac{1}{\rho}\left(\frac{\partial p_\parallel}{\partial B}\right)_{\rho,\psi} - \Delta(\rho, B, \psi)\frac{B}{\rho} \tag{19}$$

Substituting the two-temperature Maxwellian GCP plasma expressions (Eqs. (12) and (13)) into the integrability conditions (Eqs. (18) and (19)) gives a choice for enthalpy $W_{\mathrm{GCP}}(\rho, B, \psi)$ which is consistent with with the GCP theory

$$W_{\mathrm{GCP}}(\rho, B, \psi) = T_\parallel(\psi)\ln\left(\frac{\rho}{\rho_0}\frac{T_\parallel(\psi)}{T_\perp(B,\psi)}\right) + H_{\mathrm{gauge}}(\psi) \tag{20}$$

$$T_\perp(B, \psi) = \frac{BT_\parallel(\psi)}{|B - T_\parallel(\psi)\Theta(\psi)|} \tag{21}$$

for arbitrary choice of ρ_0 and H_{gauge}. The gauge transformation is possible because of the freedom to choose $(\partial W/\partial\psi)_{B,\rho}$ and is physically related to setting an arbitrary reference energy in the Bernoulli equation (Eq. (15)). With the above assumption about parallel heat transport, the system of equations is closed, and Eq. (17) is now a second-order partial differential equation fully specified by the five flux functions:

$$\{T_\parallel(\psi), H(\psi), \Omega(\psi), F(\psi), \Theta(\psi)\} \tag{22}$$

with definitions coming from Eq. (12), Eq. (15), Eq. (10), Eq. (14) and Eq. (21). The tokamak equilibrium problem has been reduced to solving Eq. (17) by fitting the flux functions (Eq. (22)) to experimental data for appropriate boundary conditions.

4. EFIT TENSOR

4.1. EFIT

Codes based on the original EFIT reconstruct the toroidal current profile from experimental measurements or given values, assuming an MHD force balance parameterisation for the current [1]. The Grad-Shafranov equation for isotropic and static cases is given by

$$\Delta^*\psi \equiv R^2\nabla\cdot\left(\frac{\nabla\psi}{R^2}\right) = -R^2p'(\psi) - FF'(\psi) \tag{23}$$

which is the limiting case of the more general system (Eq. (17)) for $\Omega(\psi) = 0$ and $\Theta(\psi) = 0$ (although toroidal flow can be approximately incorporated into 'pressure' in some codes, see appendix). The covariant representation for the field (Eq. (8)) and Ampère's law (Eq. (5)) give the identity

$$\Delta^*\psi = -RJ_\phi \tag{24}$$

which is true for any 2-D axisymmetric equilibrium. This implies a parameterisation for the toroidal current

$$J_\phi(R,\psi) = -Rp'(\psi) - FF'(\psi)/R \tag{25}$$

when isotropic and static force balance is assumed. The two flux functions are decomposed into a linear combination of basis functions with constant coefficients

$$p'(\psi) \approx \sum_{i=1}^{n_p} p_i b_{pi}(\psi) \tag{26}$$

$$FF'(\psi) \approx \sum_{i=1}^{n_f} f_i b_{fi}(\psi) \tag{27}$$

where the $b(\psi)$ represent the basis functions which are *a priori* assumed. The EFIT++ code currently supports polynomial, tension spline or Chebyshev polynomial representations. Eq. (24) is solved by alternately fitting J_ϕ to experimental or modelled constraints then performing a fast Buneman inversion [22] of

$$\Delta^*(\psi^{(n+1)}) = -RJ_\phi(R, \psi^{(n)}) \tag{28}$$

at each nth iteration. The resulting $\psi(R,Z)$ solution is completely consistent with the input $J_\phi(R,Z)$, but a recalculation of the force balance criterion Eq. (25) changes $J_\phi(R,Z)$ from the previous iteration. Thus, a self-consistent Picard iteration occurs between ψ and $J_\phi(R,\psi)$ in Eq. (28) until the change in $\psi(R,Z)$ is below an arbitrary threshold. The free flux functions are fitted to the experimental and given constraints with error by minimising

$$\chi^2 = \sum_{i=1}^{N_M} \left(\frac{M_i - C_{iM}}{\sigma_{iM}}\right)^2 + \sum_{i=1}^{N_G} \left(\frac{P_i - C_{iG}}{\sigma_{iG}}\right)^2 \tag{29}$$

where the N are the number of data points, the σ are the uncertainty, the C are the calculated values and M and P are the measured and given values respectively. In addition to the plasma currents in a tokamak, other specified, induced or unknown currents are present. When including these known, unknown and plasma currents, the calculated poloidal magnetic field at a given magnetic probe location is a superposition of current contributions through a linear combination of the current coefficients

$$\begin{aligned} C_{iM}^{(n+1)} \overset{\text{probe}}{=} & \sum_{j=\text{known}} G(\mathbf{r}_i, \mathbf{r}_j) I_j \\ & + \sum_{k=\text{free}} G(\mathbf{r}_i, \mathbf{r}_k) I_k^{(n+1)} \\ + & \int_{\text{plasma}} G(\mathbf{r}_i, \mathbf{r}) J_\phi(R, \psi^{(n)}) dRdZ \end{aligned} \tag{30}$$

where G is the response function for the probe. Other constraints are also expressed as a linear combination of the flux functions. Thus, the free coefficients and unknown currents constitute a linear least-squares problem expressible as

$$\chi^2 = \|A\mathbf{u} - \mathbf{k}\| \tag{31}$$

where $\mathbf{u}$ contains the unknown coefficients and currents, and $\mathbf{k}$ contains the constraints. This standard problem is solved in EFIT using singular value decomposition (SVD).

4.2. EFIT TENSOR system of equations

Here, we explicitly present the EFIT TENSOR system of equations in S.I. units

$$\Delta^*\psi = -\mu_0 R J_\phi \tag{32}$$

$$\begin{aligned} J_\phi = & R\frac{k}{m}\rho T_\parallel'(\psi) + \frac{1}{\mu_0 R(1-\Delta)} FF'(\psi) + \rho R^3 \Omega\Omega'(\psi) \\ & + R\rho H'(\psi) - R\left[\rho\left(\frac{\partial W}{\partial \psi}\right)_{\rho,B} + \frac{1}{\mu_0}\nabla\cdot\left(\frac{\Delta}{R^2}\nabla\psi\right)\right] \end{aligned} \tag{33}$$

$$\rho = \frac{T_\perp}{T_\parallel(\psi)}\rho_0 \exp\left(\frac{mH(\psi)}{kT_\parallel(\psi)}\right)\exp\left(\frac{mR^2\Omega^2(\psi)}{2kT_\parallel(\psi)}\right) \tag{34}$$

$$W = \frac{k}{m} T_\parallel(\psi) \log\left(\frac{\rho}{\rho_0}\frac{T_\parallel(\psi)}{T_\perp}\right) \tag{35}$$

$$T_\perp = \frac{BT_\parallel(\psi)}{\left|B - T_\parallel(\psi)\Theta(\psi)\right|} \tag{36}$$

$$\Delta \equiv \mu_0 \frac{p_\parallel - p_\perp}{B^2} \tag{37}$$

We have re-arranged Eq. (17) into an expression in J_ϕ taking advantage of the very general Eq. (24). We have also re-arranged the Bernoulli relation (Eq. (15)) into an explicit form for the mass density ρ. At fixed ρ, the current is almost a linear combination of the flux functions $T_\parallel', \Omega\Omega', FF'$ and a non-linear function of Θ. This system of equations is subject to the following identities for the five free flux functions

$$T_\parallel(\psi) = \frac{p_\parallel}{\rho}\frac{m}{k} \tag{38}$$

$$\Omega(\psi) = \frac{v_\phi}{R} \tag{39}$$

$$F(\psi) = RB_\phi\left(1 - \mu_0\frac{p_\parallel - p_\perp}{B^2}\right) \tag{40}$$

$$H(\psi) = \frac{p_\parallel}{\rho}\log\left(\frac{\rho}{\rho_0}\frac{p_\parallel}{p_\perp}\right) - \frac{1}{2}v_\phi^2 \tag{41}$$

$$\Theta(\psi) = \frac{k}{m}\rho B\left(\frac{1}{p_\parallel} - \frac{1}{p_\perp}\right) \tag{42}$$

These identities are straightforward functions of the kinetic moments $\rho, v_\phi, p_\perp, p_\parallel$ and field at any (R,Z) location. The MHD particle mass m and Boltzmann constant k are only included to give $T_\parallel$ di-

mensions of temperature, but a more useful quantity is obtained when $k = 1, m = 1$ and $T_{\|}$ has the interpretation of the ratio of parallel pressure $p_{\|}$ to mass density ρ.

4.3. Numerical scheme

The EFIT TENSOR code is a significant alteration to EFIT with a completely different set of physical assumptions, equations and free functions. However, many of the methods and constraints were adaptable to the more general case, and here we describe those adaptations.

The most important difference characteristic of the more general system is that J_ϕ (Eq. (33)) cannot in general be expressed as $J_\phi = J_\phi(R, \psi)$, nor can it be completely expressed as a linear combination of free flux functions. The problematic contributions are due to Δ, ρ and $(\partial W/\partial\psi)_{\rho,B}$. We parametrize the linear current terms and also $\Theta(\psi)$ in terms of the basis functions $b(\psi)$

$$T_{\|}'(\psi) \approx \sum_{i=1}^{n_t} t_i b_{ti}(\psi) \tag{43}$$

$$FF'(\psi) \approx \sum_{i=1}^{n_f} f_i b_{fi}(\psi) \tag{44}$$

$$\Omega\Omega'(\psi) \approx \sum_{i=1}^{n_\omega} \omega_i b_{\omega i}(\psi) \tag{45}$$

$$H'(\psi) \approx \sum_{i=1}^{n_h} h_i b_{hi}(\psi) \tag{46}$$

$$\Theta(\psi) \approx \sum_{i=1}^{n_\theta} \theta_i b_{\theta i}(\psi) \tag{47}$$

which are included in the iteration scheme

$$\begin{aligned} J_\phi^{(n+1)} &= R\frac{k}{m}\rho^{(n)}\frac{d}{d\psi}T_{\|}^{(n+1)} \\ &+ \frac{1}{\mu_0 R(1-\Delta^{(n)})}\frac{d}{d\psi}FF^{(n+1)} \\ &+ \rho^{(n)}R^3\frac{d}{d\psi}\Omega\Omega^{(n+1)} \\ &+ R\rho^{(n)}\frac{d}{d\psi}H^{(n+1)} - R\lambda^{(n+1)}\Lambda(R,Z)^{(n)} \end{aligned} \tag{48}$$

where we have introduced a non-linear plasma current $\Lambda(R, Z)$ and weighting λ corresponding to the bracketed term in Eq. (33).

$$\Lambda(R,Z) \equiv \left[\rho\left(\frac{\partial W}{\partial\psi}\right)_{\rho,B} + \frac{1}{\mu_0}\nabla\cdot\left(\frac{\Delta}{R^2}\nabla\psi\right)\right] \tag{49}$$

This contribution is treated as a new basis function computed with bi-cubic spline derivatives with an associated nuisance coefficient λ which is equal to unity for a converged solution. The reason in incorporating this non-linear term in this way instead of defining a fixed current was to allow greater flexibility for intermediate iterations at the cost of an additional degree of freedom. Forcing $\lambda = 1$ would be equivalent to specifying a known current based on the previous iteration. Contributions to the current from ρ and Δ in Eq. (48) are calculated from the previous iteration using Eqs. (34) and (37).

It is clear from Eq. (48) that, in addition to the iteration of ψ in Eq. (25), the current which satisfies force balance must also Picard iterate ρ, B and Δ contributions. Of particular concern is the exponential dependance of the density ρ on the flux functions $H, T_{\|}$, and Ω, which could conceivably produce large variation in the inferred flux functions with each iteration if not suitably constrained.

Eq. (48) is a linear expression in terms of basis functions which can be inserted into standard EFIT current constraints such as Eq. (30). In addition, the flux functions may be independently constrained using the identities in Eqs. (38)-(42). These identity constraints may be *weak* or *strong*; weak constraints depend on the kinetic moments $\rho, v_\phi, p_{\|}$, or $p_\perp$ and the intermediate calculation for B whereas strong constraints also provide B. An additional constraint should be included which specifies that $\alpha = 1$. The weighting on this condition may also be specified to aid with convergence.

An important feature of EFIT is the ability to infer the flux functions $p'(\psi)$ and $FF'(\psi)$ from the current profile. This inversion is possible due to the different R dependence in Eq. (25). However, this is not possible with the more complicated expression Eq. (48). The degeneracy of $T_{\|}'(\psi)$ and $H'(\psi)$, with each term weighted equally in R and ρ means that the columns of the linear inversion are linearly dependant and impossible to distinguish from current measurements alone. Furthermore, the anisotropy flux function $\Theta(\psi)$ has no linear contribution to the current at all, but instead influences the current through ρ and Δ. It is clear that EFIT TENSOR is a 'forward code' when invoking flow and anisotropy physics with additional information required than the usual current constraints to resolve the degeneracy. This is the price paid for the fast linear inversion of an EFIT algorithm. A non-linear least-squares fit that includes density would break this degeneracy for significant computational cost

and complexity.

To date, EFIT++ supports a number of constraints, and those that have been adapted to EFIT TENSOR are listed here for reference: vacuum toroidal field, flux loops, magnetic probes, plasma current, poloidal field coils, safety factor on axis q_0, static and rotational pressure approximations, B components, diamagnetic flux, boundary, equal ψ and Motional Stark Effect (MSE).

4.4. Dirichlet fixed-boundary mode

The magnetostatic relation Eq. (24) that is solved by EFIT at each iteration, constitutes a second-order inhomogenous partial differential equation on a finite discrete rectilinear domain with homogenous boundary conditions specified at infinity. For a given current distribution on that domain, the solution is unique. EFIT is a so-called 'free boundary' code which iterates the current distribution on this domain to give the best fit to the (usually measured) constraints and external currents. The external currents are critical to the shape of the plasma boundary on this domain.

When considering analytical solutions, such as the Soloviev solution [23], or other fixed-boundary problems, the external currents which give rise to the boundary are unknown. In particular, for the Soloviev case, the currents extend to infinity and cannot be included directly on a finite grid. For the purposes of benchmarking against an analytical solution, a fixed-boundary mode was added to EFIT TENSOR. This was done using a 'capacitance matrix' method (see for example [24]), which we will briefly describe here.

The 'capacitance matrix' method is a way of calculating what surface currents are required on an arbitrary irregular boundary to satisfy a set of boundary conditions for ψ on that boundary. Suppose we wish to solve Eq. (24) on a subdomain ω bounded by $d\omega$ with inhomogenous Dirichlet boundary conditions $\psi(s) = f(s), J_\phi(s) = 0, s \in d\omega$ for some arbitrary f. If we only care about the solution on the subdomain ω, we may solve the problem using the Green's function from the infinite domain Ω using a sequence of steps:

First, solve the inhomogenous equation for ψ_1 on Ω with boundary conditions at infinity

$$\Delta^* \psi_1 = -RJ_\phi \tag{50}$$

and obtain a new function ψ_b by measuring ψ_1 on the boundary of the subdomain $d\omega$

$$\psi_b(s) \equiv \psi_1(s), s \in d\omega \tag{51}$$

Next, define a different homogenous problem for ψ_2

$$\Delta^* \psi_2 = 0 \tag{52}$$

subject to the inhomogenous boundary condition using the function ψ_b measured before $\psi_2(s) = f(s) - \psi_b(s)$. The function $\psi_2(s)$ may be expressed completely in terms of unknown surface currents $\hat{J}_\phi(s)$ and the Green's function $G(s', s)$ on Ω

$$\begin{aligned} \psi_2(s) = \int_{d\omega} \hat{J}_\phi(s') G(s, s') ds' \\ = f(s) - \psi_b(s) \end{aligned} \tag{53}$$

For the discrete problem, the solution for the vector $\hat{J_\phi})$ may be expressed as the inversion of the response matrix G containing only the points on the boundary

$$G^{-1}(f - \psi_b) = \hat{J}_\phi \tag{54}$$

then the sum $\psi = \psi_1 + \psi_2$ uniquely satisfies the inhomogenous Dirichlet boundary conditions $\psi(s) = f(s), J_\phi(s) = 0, s \in d\omega$ on ω and the fixed boundary problem is solved.

In the current implementation of EFIT TENSOR, the user specifies which grid points constitute the boundary and what the value of ψ is on each grid point. Since the continuous boundary will not, in general, cross the grid points, the values at the grid points may vary accordingly. The last closed flux surface search is also disabled and specified as the supplied boundary. Fig. 1 is an example fixed-boundary solution using this method. The ψ contours inside the limiter region correspond to the Soloviev solution, and the contours outside the limiter are a by-product of the method and of no interest.

5. Tests

5.1. Extension of Soloviev solution

The Soloviev solution is an analytical solution to the Grad-Shafranov equation when $p(\psi)$ and $F^2(\psi)$ in Eq. (23) are linear functions of ψ. Adopting a

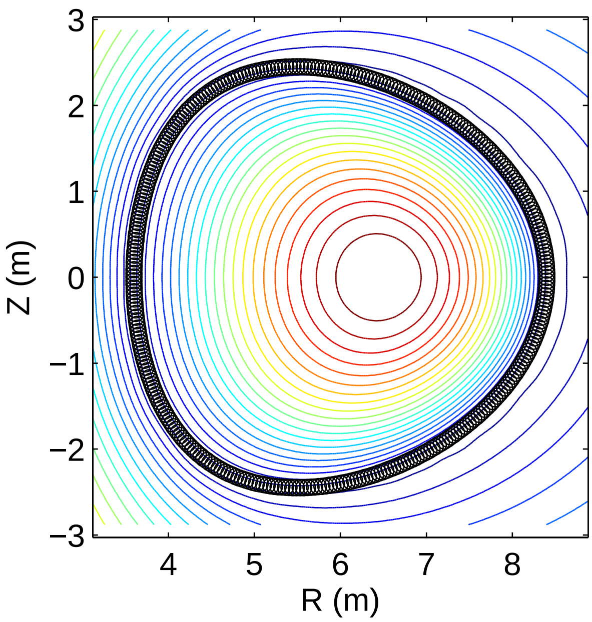

Figure 1: A Soloviev solution as reconstructed with EFIT TENSOR using a fixed-boundary mode.

useful form used by [25], the solution can be expressed as

$$\bar{\psi} = \left[x - \frac{1}{2}\epsilon\left(1 - x^2\right)\right]^2 + \left(1 - \frac{1}{4}\epsilon^2\right)\left[1 + \epsilon\tau x\left(2 + \epsilon x\right)\right]\left(\frac{y}{\sigma}\right)^2 \quad (55)$$

$$\psi = \left(\frac{a^2 B_0}{\alpha}\right)\bar{\psi} \quad (56)$$

$$R = ax + R_0 \quad (57)$$

$$Z = ay \quad (58)$$

$$p_S(\bar{\psi}) = p'[1 - \bar{\psi}] \quad (59)$$

$$F_S^2(\bar{\psi}) = F'^2[1 - \bar{\psi}] + R_0^2 B_0^2 \quad (60)$$

where $\{\epsilon, \sigma, \tau\}$ control the shape of the ψ solution and are known as the inverse aspect ratio, ellipticity and triangularity respectively. The field scaling is controlled by α and B_0. The linear profiles $\{p_S, F_S^2\}$ correspond to the static and isotropic flux functions and their gradients $\{p', F'^2\}$ depend on the above parameters. To make the simplest possible extension to flow and anisotropy, we re-write the Grad-Shafranov equation as

$$p_\perp = p_\perp(R, B, \psi) \quad (61)$$

$$\nabla \cdot \left[\left(\frac{\nabla\psi}{R^2}\right)\right] - \frac{F^2}{(1-\Delta)^2}\nabla_\psi \log(1-\Delta) = -\frac{1}{(1-\Delta)}\left(\frac{\partial p_\perp}{\partial\psi}\right)_{B,R} - \frac{F(\psi)F'(\psi)}{R^2(1-\Delta)^2} \quad (62)$$

$$\left(\frac{\partial p_\perp}{\partial R}\right)_{\psi,B} = \rho R \Omega(\psi)^2 \quad (63)$$

$$\left(\frac{\partial p_\perp}{\partial B}\right)_{\psi,R} = -\Delta B \quad (64)$$

If we wish to maintain the same ψ geometry for our flow and anisotropy solution as for the Soloviev solution, then the partial derivatives of $p_\perp$ and F with respect to ψ in Eq. (62) must be the same, whilst also satisfying the additional conditions (Eqs. (63) and (64)). By inspection, this is achieved with the profiles

$$p_\perp(R, B, \psi) = \frac{1}{2}\rho_0\Omega_0^2 R^2 - \frac{\Delta_0}{2}B^2 + \sigma_0 p_S(\psi) \quad (65)$$

$$p_\parallel(R, B, \psi) = \frac{1}{2}\rho_0\Omega_0^2 R^2 + \frac{\Delta_0}{2}B^2 + \sigma_0 p_S(\psi) \quad (66)$$

$$F^2(\psi) = \sigma_0^2 F_S^2(\psi) \quad (67)$$

where $\Omega_0, \sigma_0 \equiv 1 - \Delta_0, \rho_0$ are constants with respect to R, B, ψ. On substitution of these expressions into Eq. (62), the logarithmic second term disappears and we re-obtain the ordinary Grad-Shafranov equation and the usual Soloviev solution. It is interesting to note that this implies that flow and/or anisotropy shear are the required properties to alter the current profile and magnetic topology of the analytical solution.

There are advantages and disadvantages to this solution; although this solution exhibits the important de-coupling of magnetic surfaces and pressure surfaces, it does not do so with any respect for transport physics or thermodynamic assumptions. More specifically, one cannot write the pressures as $p_\parallel(\rho, B, \psi) = \rho T_\parallel(\psi)$ and $p_\perp(\rho, B, \psi) = \rho T_\perp(B, \psi)$ as assumed in EFIT TENSOR as discussed earlier. For example, dividing Eq. (65) by density ρ_0 will give $T_\perp = T_\perp(R, B, \psi)$. This is interesting because it implies that the inclusion of flow and anisotropy in equilibrium introduces energy transport into the force balance inference problem. A related effect has been noted previously [2] when considering the direction of density shift for different enthalpy assumptions. It is, therefore, to be expected that

when using this analytical solution as a constraint, the physical assumptions of the parallel heat transport model will prevent the same solution being obtained.

5.2. *Comparison to analytical solution*

5.2.1. *Force balance convergence*

A series of force balance numerical benchmarks were carried out on EFIT TENSOR by constraining to analytical Soloviev solutions and testing force balance of the resulting solution. A 2-point finite-difference comparison between the left and right hand sides of the fluid force equation (Eq. (1)) was used to measure force balance error. The linear current profile of the Soloviev solution meant that this force balance test was found to be accurate to $1\times\ 10^{-14}$ when the analytical solution was tested with the same scripts. The parameters used for the analytical constraints are shown in Table 1. The ordinary tokamak parameters such as field strength, plasma current and geometry were chosen to resemble an ITER like configuration, and the kinetic properties of flow, mass density and anisotropy were chosen to maximize the changes to the analytical pressure from the ordinary case whilst still converging for the same numerical options such as grid resolution and polynomial order. The results of the force balance benchmark are presented in Fig. 2. The figure shows that the code accuracy scales equally well for static, flowing and anisotropic cases, with near identical accuracy for flow and static cases. The anisotropic cases were approximately 3 times worse than the static and flow cases, which is likely due to the spline derivatives used for the non-linear current calculation of $\nabla\cdot\left(\frac{\Delta}{R^2}\nabla\psi\right)$. Better numerical evaluations of this term are perhaps possible, but have not been pursued in this work.

Table 1: Extended Soloviev solution parameters

ϵ	0.4
σ	1
τ	1
R_0	6 m
B_0	5 T
α	-3
ρ_0	$1\times\ 10^{-7}$
Ω_0	0 or $7\times\ 10^{5}$rad s^{-1}
Δ_0	0 or $4\times\ 10^{-3}$
I_p	16 MA
q^*	1.6
β_p	1.0
β_T	0.07

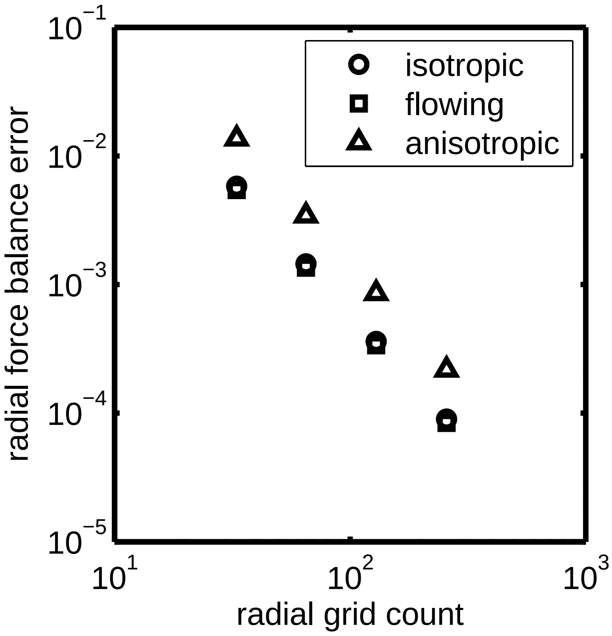

Figure 2: Comparison between plasma and field force balance at the geometric axis for extended Soloviev solutions. The parameters used for these cases are shown in Table 1.

5.2.2. *Analytical solution reconstruction*

In this section, we compare the reconstructed solutions to the analytical solutions for the three cases of static isotropic, flowing and anisotropic plasma. All three analytical solutions were generated on a 257×257 grid. Kinetic moments of $p_{\|}, p_{\perp}, v_{\phi}$ and ρ were taken from the generated analytical solutions and used as input constraints for EFIT TENSOR. For the ordinary static case, the only free function was $T'_{\|}$ with $n_t = 1$ the order of the polynomial. For the flowing case, H' was required for convergence and was set to $n_h = 2$. For the anisotropic case, Θ' was required instead, also with order $n_\theta = 2$. These were the minimal order polynomials found to converge total ψ to better than $1\times\ 10^{-15}$, $1\times\ 10^{-11}$ and $1\times\ 10^{-7}$ for the ordinary, flowing and anisotropic cases respectively.

A comparison of reconstructed radial current and pressure profiles is given in Fig. 3 for each of the

three cases. The only constraint required to obtain the static case was total current, whereas the flowing and anisotropic cases had identity constraints for $T_{\|}, \Omega, H$ and Θ using Eqs. (38) and (42). No current or field profile data was used as an input in any case. The pressure profiles in Fig. 3 show very good agreement; in the isotropic case, this is due to the uniqueness of equilibrium for a given current scaling assuming a linear pressure form.

In the flow case, pressure was constrained, so it is unremarkable that the pressure profiles agree, however what is remarkable is that the pressure is displaced whilst the magnetic surfaces remain unchanged, as expected for large flows (corresponding to sonic Mach number ~ 0.8 and Alvén Mach number $\sim 0.2-0.8$ across the midplane). Fig. 4 is a plot of the EFIT TENSOR solution clearly showing the pressure displacement, whilst correctly satisfying force balance in Fig. 2. As the flow increases with radius, the agreement between the reconstructed current and the analytical solution diverges as the heat flow assumption $T = T(\psi)$ becomes less relevant to the analytical case.

The anisotropic case shows similar unremarkably good agreement for the constrained pressure, but a significant change is observed in the current profile. The disturbance is symmetric in poloidal flux ψ and is a direct consequence of the unphysical B^2 dependence on $T_{\|}$ in the analytical solution. Both the analytic solution and the EFIT TENSOR solution satisfy force balance but for different parallel heat flow assumptions in Eq. (17). This demonstrates that even with very good agreement for pressure profiles, the inferred magnetic topology can be radically different when considering anisotropy (even between anisotropy models), a result which qualitatively agrees with previous findings on q profile in the presence of anisotropy [11, 6]. Conversely, it follows that any pressure inferred from a measured magnetic topology must be done so after careful consideration of the plasma transport and anisotropy to be physically relevant.

5.3. MAST TRANSP constraints

An equilibrium reconstruction was performed for MAST discharge 18696 at 290 ms using standard MAST EFIT++ magnetic constraints; magnetic probe, flux loops, field and induced coil currents and total plasma current. Motional Stark Effect measurements were unavailable for this shot. In addition to the usual constraints, identity constraints on $p_{\|}, p_{\perp}, v_{\phi}, \rho$ were provided from TRANSP [26] to

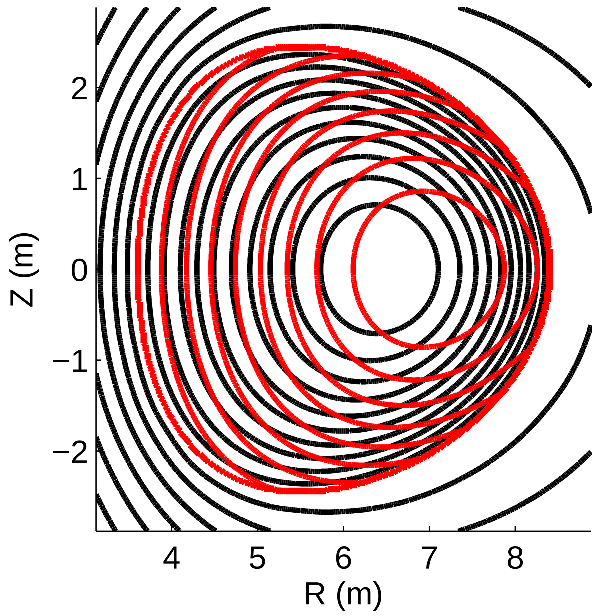

Figure 4: The displacement of pressure contours from magnetic surfaces in the reconstructed flowing Soloviev benchmark. Pressure shown in red.

constrain the five flux functions, thereby including full anisotropy and flow in the force balance. The conversion from equivalent documented TRANSP quantities was performed as (ignoring the CGS unit conversion)

$$v_{\phi} = R \times \text{OMEGA} \quad (68)$$

$$\rho = \text{NI} \times m_i + \text{a.m.u.} \times \text{AIMP} \times \text{NIMP} \quad (69)$$

$$p_{\|} = \text{PPLAS+2}\times\text{UFASTPA} \quad (70)$$

$$p_{\perp} = \text{PPLAS+UFASTPP} \quad (71)$$

where NI, AIMP, NIMP, OMEGA, PPLAS, UFASTPA and UFASTPP are: total ion density, average impurity mass and density, toroidal angular velocity, total thermal pressure, fast ion parallel and perpendicular energies. These TRANSP values were mapped to the mid-plane as functions of major radius. The resulting best fit is shown in Fig. 5. The largest discrepancy between TRANSP and EFIT TENSOR in this example is evident in the centrifugal force balance. Even though density and rotation were prescribed, an EFIT TENSOR solution with a lower rotation was inferred. This is likely related to the density being prescribed as a flux function in TRANSP, and the consequent density symmetry in radial mapping. The 2-D

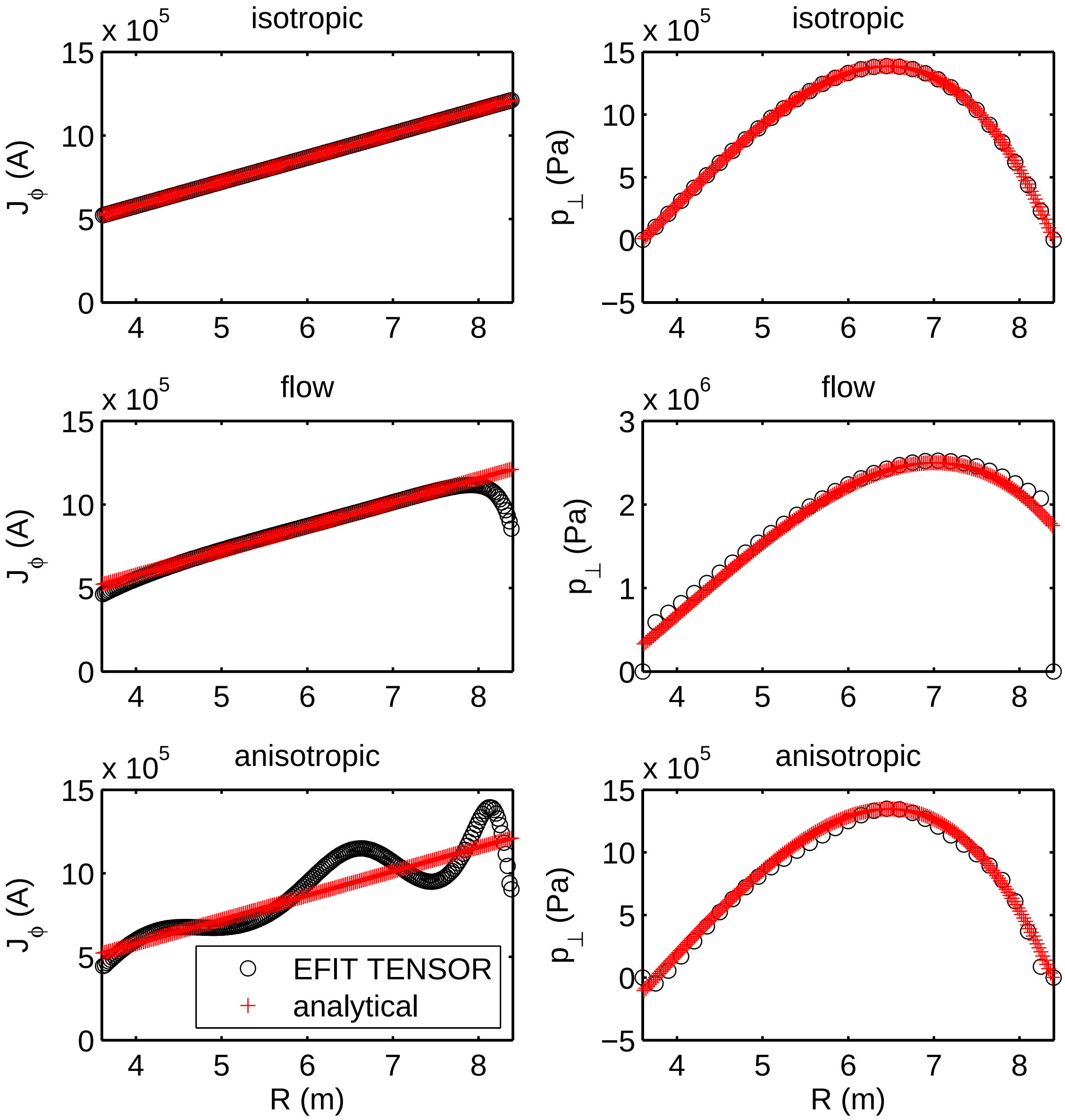

Figure 3: Reconstruction of analytical radial profiles using EFIT TENSOR and constraining to pressure. The difference in parallel heat transport assumptions of the analytical solution and the two temperature GCP model has resulted in a different current profile for the same pressure profile.

TRANSP field variables BR, BZ and BPHI were extracted and used in a radial force balance benchmark similar to that used in previously in this paper (Fig. 6). The force balance test in Fig. 6 shows that, for this example, TRANSP underestimates the plasma pressure contribution either side of the magnetic axis and that MHD equilibrium with flow and anisotropy is not satisfied away from the magnetic axis. A discrepancy is not surprising since TRANSP only uses a rotational pressure approximation and takes beam pressure to be the average of parallel and perpendicular components, but the magnitude of the error is interesting. The additional structure in the TRANSP force profile is due to the flat spots in the assumed TRANSP pressure profile in Fig. 5, which is not replicated with the second order polynomial used in this EFIT TENSOR example.

We have thus demonstrated an equilibrium reconstruction of a real MAST discharge including flow and anisotropy corrections to full order using measurements of radial profiles taken from TRANSP. We anticipate, in future work, to replace many of these constraints with experimental measurements of density, rotation and temperature.

6. Conclusion

A new force model for EFIT has been presented which includes full order toroidal flow and anisotropy effects under the assumptions of ideal MHD for a single fluid guiding centre plasma. The parallel transport model assumed is that parallel temperature is a flux function. This model has been demonstrated and tested in the existing code EFIT++ and was found to produce identical results in the static and isotropic limits with a comparable computational cost. The model was also tested for force balance using a finite difference scheme and was benchmarked against an analytical solution. It was found that significant differences in the inferred current are possible for the same kinetic plasma constraints which result from the choice of parallel heat transport model. This implies that for sufficiently anisotropic plasma, the parallel transport model can be compared against measured current profiles, providing a novel measure of heat flow from equilibrium constraints.

In future work, we will investigate the effects of flow and anisotropy on MAST shots using EFIT TENSOR. We anticipate that rotation and density constraints will be measured from experiment,

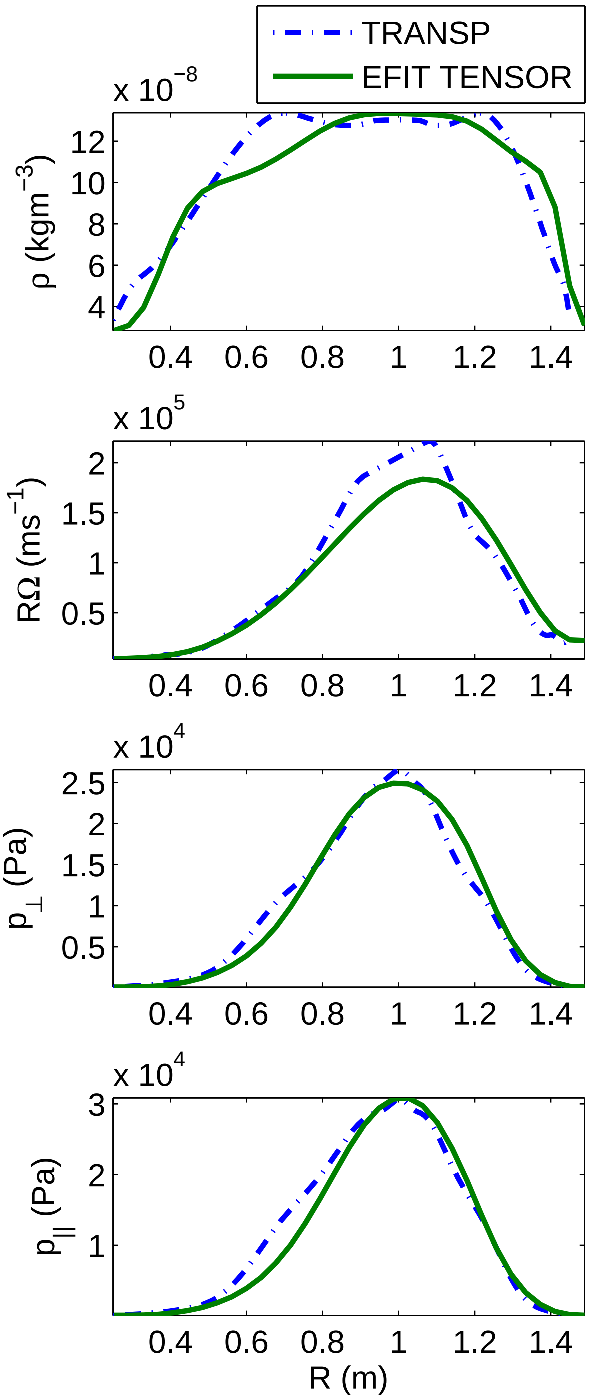

Figure 5: Reconstructed radial profiles for MAST18696 at 290ms.

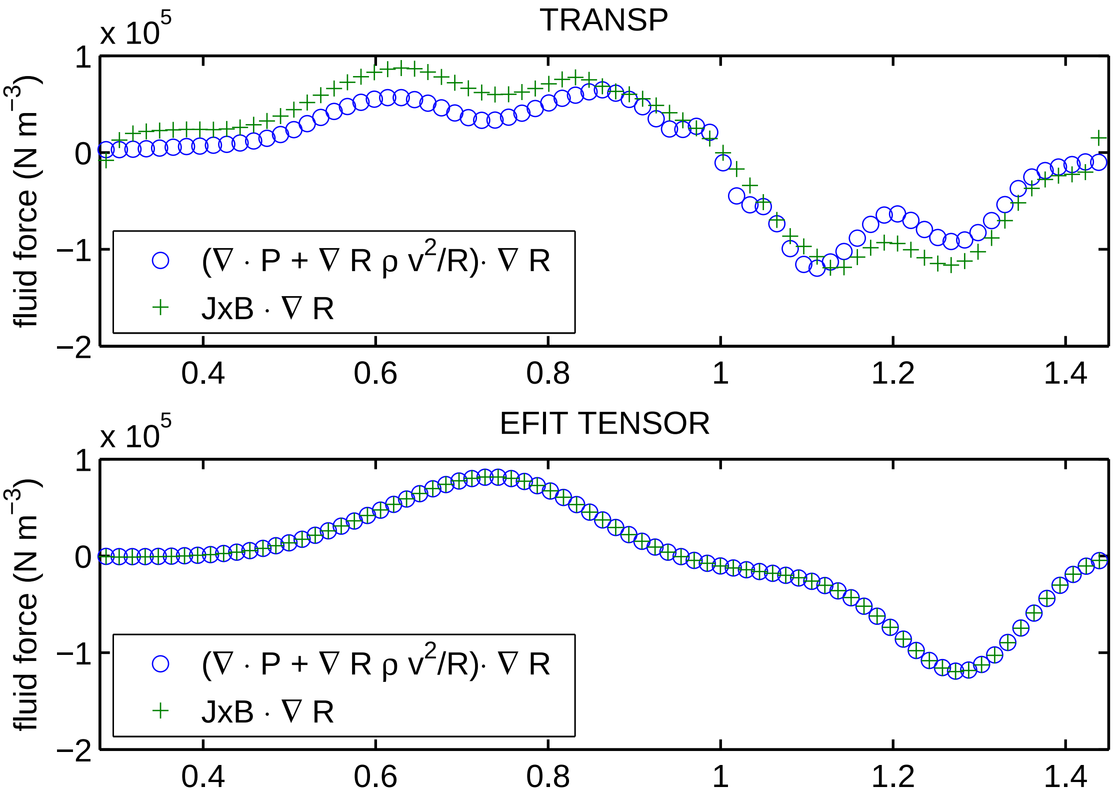

Figure 6: Finite difference radial force balance check for profiles produced by TRANSP and EFIT TENSOR, with the inclusion of full order flow and anisotropy, for MAST discharge 18696 @ 290ms.

and parallel and perpendicular pressures will be calculated using an NBI particle model such as NUBEAM [27] or LOCUST [28].

7. Appendix

7.1. *Reduction of modified Grad-Shafronov equation to isotropic and/or static cases*

It is instructive to consider the reduction of the more general equilibrium problem to simpler cases, and the corresponding reduction in the number of free parameters. Indeed, treatments including poloidal flow have a free flux function in addition to the five presented in this work (but, it should be noted, for a different expression of $W(\rho, B, \psi)$ [2, 15]).

Setting $\Delta \equiv 0$ in Eq. (17) gives the isotropic force balance problem for toroidal flow

$$\nabla \cdot \left[\left(\frac{\nabla\psi}{R^2} \right) \right] = -\rho T'(\psi) - \rho H'(\psi) + \rho \left(\frac{\partial W}{\partial \psi} \right)_\rho - \frac{F(\psi)F'(\psi)}{R^2} + \rho R^2 \Omega(\psi)\Omega'(\psi) \tag{72}$$

$$H(\psi) = T(\psi) \ln \left(\frac{\rho}{\rho_0} \right) - \frac{1}{2} R^2 \Omega(\psi)^2 \tag{73}$$

$$W(\rho, \psi) = T(\psi) \ln \left(\frac{\rho}{\rho_0} \right) \tag{74}$$

$$\{T(\psi), H(\psi), \Omega(\psi), F(\psi)\} \tag{75}$$

which is the form found by many authors [18, 19, 20, 21] . A consequence of Eq. (73) is another widely known and useful form for this system

$$\nabla \cdot \left[\left(\frac{\nabla\psi}{R^2} \right) \right] = -\left(\frac{\partial p}{\partial \psi} \right)_R - \frac{F(\psi)F'(\psi)}{R^2} \tag{76}$$

$$\left(\frac{\partial p}{\partial R} \right)_\psi = \rho R \Omega(\psi)^2 \tag{77}$$

$$p(R, \psi) \equiv \rho(R, \psi) T(\psi) \tag{78}$$

$$\{p(R, \psi), \Omega(\psi), F(\psi)\} \tag{79}$$

If we further assume zero flow by setting $\Omega(\psi) \equiv 0$ in Eq. (17) then, on re-examination of Eq. (73), we identify no more explicit radial dependence and a redundant separation of temperature and density. Thus, we arrive at the basic Grad-Shafranov equation

$$\nabla \cdot \left[\left(\frac{\nabla\psi}{R^2} \right) \right] = -p'(\psi) - \frac{F(\psi)F'(\psi)}{R^2} \tag{80}$$

$$H(\psi) = T(\psi) \ln \left(\frac{\rho(\psi)}{\rho_0} \right) \tag{81}$$

$$p(\psi) \equiv \rho(\psi) T(\psi) \tag{82}$$

$$\{p(\psi), F(\psi)\} \tag{83}$$

Conversely, the purely anisotropic system becomes

$$\nabla \cdot \left[(1-\Delta) \left(\frac{\nabla\psi}{R^2} \right) \right] = -\rho T_\parallel'(\psi) - \rho H'(\psi) + \rho \left(\frac{\partial W}{\partial \psi} \right)_{B,\rho} - \frac{F(\psi)F'(\psi)}{R^2(1-\Delta)} \tag{84}$$

$$H(\psi) = T_\parallel(\psi) \ln \left(\frac{\rho}{\rho_0} \frac{T_\parallel(\psi)}{T_\perp(B, \psi)} \right) \tag{85}$$

$$W(\rho, B, \psi) = T_\parallel(\psi) \ln \left(\frac{\rho}{\rho_0} \frac{T_\parallel(\psi)}{T_\perp(B, \psi)} \right) \tag{86}$$

$$T_\perp(B, \psi) = \frac{B T_\parallel(\psi)}{\left| B - T_\parallel(\psi)\Theta(\psi) \right|} \tag{87}$$

$$\left\{ T_\parallel(\psi), H(\psi), F(\psi), \Theta(\psi) \right\} \tag{88}$$

and analogous to the pure flow case, we perform the full ψ derivative of the Bernoulli equation and using the integrability relations (Eqs. (18) and (19)) we obtain a similar set of equations

$$\nabla \cdot \left[(1-\Delta) \left(\frac{\nabla\psi}{R^2} \right) \right] = -\left(\frac{\partial p_\parallel}{\partial \psi} \right)_B - \frac{F(\psi)F'(\psi)}{R^2(1-\Delta)} \tag{89}$$

$$\left(\frac{\partial p_\parallel}{\partial B} \right)_\psi = -\Delta B \tag{90}$$

$$p_\parallel(B, \psi) \equiv \rho(B, \psi) T_\parallel(\psi) \tag{91}$$

$$\left\{ p_\parallel(B, \psi), \Theta(\psi), F(\psi) \right\} \tag{92}$$

which reduces immediately to the form given by Grad[17].

7.2. *Rotational pressure approximation*

Here we relate our set of free functions (Eq. (22)) to the ‘rotational pressure’ approximation used in some existing codes. Working in S.I. units, the definition of rotational pressure is through an expansion in major radius

$$\left(\frac{\partial p_\parallel}{\partial \psi} \right)_R \approx P'_{\mathrm{axis}}(\psi) + x P'_{\mathrm{rot}}(\psi) \tag{93}$$

$$x \equiv \left(\frac{R^2}{R_0^2} - 1 \right) \tag{94}$$

where R_0 is some origin (ideally, the magnetic axis). Casting the isotropic pressure in terms of x and Taylor expanding around $x = 0$ gives the required definitions

$$p_{\|}(x, B, \psi) = \rho_0 \frac{k}{m} \frac{B}{|B - \Theta(\psi) T_{\|}(\psi)|} \times T_{\|}(\psi) \exp\left(\frac{mH(\psi)}{kT_{\|}(\psi)}\right) \times \exp\left(\frac{mR_0^2(x+1)\Omega(\psi)^2}{2kT_{\|}(\psi)}\right) \quad (95)$$

$$D_{\text{axis}}(\psi) \equiv \rho_0 \frac{B}{|B - \Theta(\psi) T_{\|}(\psi)|} \exp\left(\frac{mH(\psi)}{kT_{\|}(\psi)}\right) \times \exp\left(\frac{mR_0^2\Omega(\psi)^2}{2kT_{\|}(\psi)}\right) \quad (96)$$

$$P_{\text{axis}}(\psi) \equiv \frac{k}{m} T_{\|}(\psi) D_{\text{axis}}(\psi) \quad (97)$$

$$P_{\text{rot}}(\psi) \equiv \frac{1}{2} R_0^2 \Omega(\psi)^2 D_{\text{axis}}(\psi) \quad (98)$$

which is clearly only strictly appropriate for $\Theta(\psi) = 0$, i.e.: when the system is isotropic.

8. Acknowledgments

The first author would like to thank Luca Guazzotto (University of Rochester), Greg von Nessi (ANU), Rob Akers and Ken McClements (CCFE) for very useful discussions at various points in this research, and David Muir (CCFE) and David Pretty (ANU) for invaluable assistance with MAST data access. This work was funded by the Australian Research Council through Grant Nos. DP1093797 and FT0991899 and by the RCUK Energy Programme under Grant No. EP/I501045 and the European Communities under the contract of Association between EURATOM and CCFE. The views and opinions expressed herein do not necessarily reflect those of the European Commission.

References

[1] L. Lao, H. John, R. Stambaugh, A. Kellman, W. Pfeiffer, Reconstruction of current profile parameters and plasma shapes in tokamaks, Nuclear Fusion 25 (11) (1985) 1611–1622.

[2] R. Iacono, A. Bondeson, F. Troyon, R, Axisymmetric toroidal equilibrium with flow and anisotropic pressure, Physics of Fluids B.

[3] L. Appel, G. Huysmans, L. Lao, P. McCarthy, D. Muir, E. Solano, J. Storrs, D. Taylor, W. Zwingmann, A Unified Approach to Equilibrium Reconstruction, in: Proceedings of the 33rd EPS Conference, no. 06, Rome, 2006.

[4] A. Fasoli, C. Gormenzano, H. Berk, B. Breizman, S. Briguglio, D. Darrow, N. Gorelenkov, W. Heidbrink, A. Jaun, S. Konovalov, Others, Chapter 5 : Physics of energetic ions, Nuclear Fusion 47 (6) (2007) 264.

[5] W. Cooper, G. Bateman, D. Nelson, T. Kammash, Beam-induced tensor pressure tokamak equilibria, Nuclear Fusion 20 (1980) 985–992.

[6] M. J. Hole, G. von Nessi, M. Fitzgerald, K. G. McClements, J. Svensson, Identifying the impact of rotation, anisotropy, and energetic particle physics in tokamaks, Plasma Physics and Controlled Fusion 53 (7) (2011) 074021. doi:10.1088/0741-3335/53/7/074021.

[7] L. Guazzotto, R. Betti, J. Manickam, S. Kaye, Numerical study of tokamak equilibria with arbitrary flow, Physics of Plasmas 11 (2) (2004) 604. doi:10.1063/1.1637918.

[8] M. J. Hole, G. Dennis, Energetically resolved multiple-fluid equilibria of tokamak plasmas, Plasma Physics and Controlled Fusion 51 (3) (2009) 035014. doi:10.1088/0741-3335/51/3/035014.

[9] M. Fitzgerald, S. Sharapov, M. Hole, High-β equilibria in tokamaks with toroidal flow, Physics of Plasmas 18 (9) (2011) 092508. doi:10.1063/1.3641966.

[10] V. D. Pustovitov, Anisotropic pressure effects on plasma equilibrium in toroidal systems, Plasma Physics and Controlled Fusion 52 (6) (2010) 065001. doi:10.1088/0741-3335/52/6/065001.

[11] W. Zwingmann, L. Eriksson, P. Stubberfield, Equilibrium analysis of tokamak discharges with anisotropic pressure, Plasma Physics and Controlled Fusion 43 (2001) 1441.

[12] H. Grad, The Guiding Center Plasma, Proceedings of Symposia in Applied Mathematics 18 (1966) 162–247.

[13] D. Dobrott, J. Greene, Steady Flow in the Axially Symmetric Torus Using the Guiding-Center Equations, Physics of Fluids 13 (1970) 2391.

[14] P. M. Bellan, Fundamentals of plasma physics, Cambridge University Press, Cambridge, 2006.

[15] H. de Blank, Theory of the m= 1 kink mode in toroidal plasmas, Ph.D. thesis, Rijksuniversiteit Utrecht (1990).

[16] H. Grad, H. Rubin, Proceedings of the second United Nations international conference on the peaceful uses of atomic energy, in: Nuclear Physics, Vol. 14, 1958, p. 400. doi:10.1016/0029-5582(59)90092-6.

[17] H. Grad, Toroidal containment of a plasma, Physics of Fluids.

[18] R. Lovelace, C. Mehanian, C. Mobarry, M. Sulkanen, Theory of axisymmetric magnetohydrodynamic flows-disks, The Astrophysical Journal Supplement Series 62 (1986) 1–37.

[19] H. Zehrfeld, B. Green, Stationary toroidal equilibria at finite beta(One-fluid MHD model for beta and flow effects on stationary axisymmetric self consistent toroidal equilibria, using Bennett relation), Nuclear Fusion 12 (1972) 569–575.

[20] S. Semenzato, R. Gruber, H. Zehrfeld, Computation of symmetric ideal MHD flow equilibria, Computer Physics reports 1 (7-8) (1984) 389–425. doi:10.1016/0167-7977(84)90011-X.

[21] E. Hameiri, The equilibrium and stability of rotating plasmas, Physics of Fluids 26 (1983) 230.

[22] K. Lackner, Computation of ideal mhd, Computer Physics Communications 12 (1) (1976) 33–44.

[23] L. Solov'ev, Hydromagnetic stability of closed plasma configurations, Reviews of Plasma Physics 6 (1975) 239.

[24] W. Proskurowski, O. Widlund, On the Numerical Solution of Helmholtz's Equation by the Capacitance Matrix Method, Mathematics of Computation.

[25] J. Goedbloed, R. Keppens, S. Poedts, Advanced magnetohydrodynamics: with applications to laboratory and astrophysical plasmas, Cambridge Univ Pr, 2010.

[26] R. Hawryluk, An empirical approach to tokamak transport, in: Physics of plasmas close to thermonuclear conditions, CEC, Brussels, 1980, Varenna, Italy, 1979.

[27] A. Pankin, The tokamak Monte Carlo fast ion module NUBEAM in the National Transport Code Collaboration library, Computer Physics Communications 159 (3) (2004) 157–184. `doi:10.1016/j.cpc.2003.11.002`.

[28] R. Akers, L. Appel, P. Carolan, N. Conway, G. Counsell, M. Cox, S. Gee, M. Gryaznevich, R. Martin, A. Morris, M. Nightingale, A. Sykes, M. Mironov, M. Walsh, Neutral beam heating in the START spherical tokamak, Nuclear Fusion 122.